Progress In Electromagnetics Research B, Vol. 8, 257–292, 2008

APPLYING SHANNON WAVELET BASIS FUNCTIONS TO THE METHOD OF MOMENTS FOR EVALUATING THE RADAR CROSS SECTION OF THE CONDUCTING AND RESISTIVE SURFACES

R. Danesfahani and S. Hatamzadeh-Varmazyar

Department of Electrical Engineering
Islamic Azad University
Science and Research Branch, Tehran, Iran

E. Babolian

Department of Mathematics
Tarbiat Moallem University
599 Taleghani Avenue, Tehran 15618, Iran

Z. Masouri

Department of Mathematics
Islamic Azad University
Science and Research Branch, Tehran, Iran

Abstract—In this paper, we apply the Shannon wavelet basis functions to the method of moments to evaluate the radar cross section (RCS) of the conducting and resistive surfaces. The problem is modeled by the integral equations of the first or second kind. An effective numerical method for solving these problems based on the moments method and using Shannon wavelet basis functions is proposed. The validity and accuracy of the method is checked on some examples, and the Shannon wavelets are compared with the well-known block-pulse functions (BPFs) from the viewpoint of computational efficiency. The problem of evaluating the RCS is treated in detail, and illustrative computations are given for some cases. This method can be generalized to apply to objects of arbitrary geometry and arbitrary material.

1. INTRODUCTION

The development of numerical methods for solving integral equations in Electromagnetics has attracted intensive researches for more than four decades [1, 2]. The use of high-speed computers allows one to make more computations than ever before. During these years, careful analysis has paved the way for the development of efficient and effective numerical methods and, of equal importance, has provided a solid foundation for a through understanding of the techniques.

Over several decades, electromagnetic scattering problems have been the subject of extensive researches (see [3–54] and their references). Scattering from arbitrary surfaces such as square, cylindrical, circular, spherical [3–9] are commonly used as test cases in computational Electromagnetics, because analytical solutions for scattered fields can be derived for these geometries [3].

An important parameter in scattering studies is the electromagnetic scattering by a target which is usually represented by its echo area or radar cross section (RCS) [55]. The echo area or RCS is defined as the area intercepting the amount of power that, when scattered isotropically, produces at the receiver a density that is equal to the density scattered by the actual target [56]. For a two-dimensional target the scattering parameter is referred to as the scattering width (SW) or alternatively as the radar cross section per unit length.

When the transmitter and receiver are at the same location, the RCS is usually referred to as monostatic and it is referred to as bistatic when the two are at different locations [55]. Observations made toward directions that satisfy Snell's law of reflection are usually referred to as specular. Therefore the RCS of target is very important parameter which characterizes its scattering properties. A plot of the RCS as a function of the space coordinates is usually referred to as the RCS pattern.

Evaluating the radar cross section of the conducting or resistive surfaces leads to solve the integral equations of the first or second kind. For solving these integral equations, several numerical approaches have been proposed [57, 58]. These numerical methods often use the basis functions and transform the integral equation to a linear system that can be solved by direct or iterative methods [57]. It is important in these methods to select an appropriate set of basis functions so that the approximate solution of integral equation has a good accuracy.

It is the purpose of this paper to use a set of orthogonal basis functions called Shannon wavelets and to apply them to the method of moments to evaluate the RCS of the conducting or resistive surfaces. Using this method, the first or second kind integral equation reduces

to a linear system of algebraic equations. Solving this system gives an approximate solution for these problems.

First of all, the electric field integral equation is introduced. After this, an extensive review of wavelets containing the definition and expansion is performed. Then, the method of moments is proposed for solving the mentioned integral equations using Shannon wavelet basis functions. The validity and accuracy of the method is checked on some examples, and the Shannon wavelets are compared with the well-known block-pulse functions from the viewpoint of computational efficiency. Finally, the RCS problem is described in detail and solved by the presented method, and illustrative computations are given to complete the procedure.

2. ELECTRIC AND MAGNETIC FIELD INTEGRAL EQUATIONS

The key to the solution of any scattering problem is a knowledge of the physical or equivalent current density distributions on the volume or surface of the scatterer. Once these are known then the radiated or scattered fields can be found using the standard radiation integrals. A main objective then of any solution method is to be able to predict accurately the current densities over the scatterer. This can be accomplished by the integral equation (IE) method [55].

In general there are many forms of integral equations. Two of the most popular for time-harmonic Electromagnetics are the electric field integral equation (EFIE) and the magnetic field integral equation (MFIE). The EFIE enforces the boundary condition on the tangential electric field and the MFIE enforces the boundary condition on the tangential components of the magnetic field. The electric field integral equation will be discussed here.

2.1. Electric Field Integral Equation

The electric field integral equation (EFIE) is based on the boundary condition that the total tangential electric field on a perfectly electric conducting (PEC) surface of scatterer is zero [55]. This can be expressed as

$$\mathbf{E}_t^{\mathrm{t}}(\mathbf{r}=\mathbf{r}_s)=\mathbf{E}_t^{\mathrm{inc}}(\mathbf{r}=\mathbf{r}_s)+\mathbf{E}_t^{\mathrm{scat}}(\mathbf{r}=\mathbf{r}_s)=0 \quad \text{on } S, \tag{1}$$

or

$$\mathbf{E}_t^{\mathrm{scat}}(\mathbf{r}=\mathbf{r}_s)=-\mathbf{E}_t^{\mathrm{inc}}(\mathbf{r}=\mathbf{r}_s) \quad \text{on } S, \tag{2}$$

where, S is the conducting surface of the scatterer and $\mathbf{r} = \mathbf{r}_s$ is the position vector of any point on the surface of the scatterer. The subscript t indicates tangential components.

The incident field that impinges on the surface of the scatterer induces on it an electric current density $\mathbf{J}_s$ which in turn radiates the scattered field. The scattered field everywhere can be found using the following equation [55]:

$$\mathbf{E}^{\text{scat}}(\mathbf{r}) = -j\omega\mathbf{A} - j\frac{1}{\omega\mu\epsilon}\nabla(\nabla\cdot\mathbf{A}) = -j\frac{1}{\omega\mu\epsilon}\left[\omega^2\mu\epsilon\mathbf{A} + \nabla(\nabla\cdot\mathbf{A})\right], \tag{3}$$

where:

ϵ, is the permittivity of the medium;
μ, is the permeability of the medium;
ω, is the angle frequency of the incident field;
∇, is the gradient operator;
$\mathbf{A}$, is the magnetic vector potential, so that

$$\mathbf{A}(\mathbf{r}) = \mu\int\int_S \mathbf{J}_s(\mathbf{r}')\frac{e^{-j\beta R}}{4\pi R}ds', \tag{4}$$

where, R is the distance from source point to the observation point.

Equations (3) and (4) can also be expressed as [55]

$$\mathbf{E}^{\text{scat}}(\mathbf{r}) = -j\frac{\eta}{\beta}\left[\beta^2\iint_S \mathbf{J}_s(\mathbf{r}')G(\mathbf{r},\mathbf{r}')ds' + \nabla\iint_S \nabla'\cdot\mathbf{J}_s(\mathbf{r}')G(\mathbf{r},\mathbf{r}')ds'\right], \tag{5}$$

where, η is the intrinsic impedance of the medium and β is the phase constant; $\mathbf{r}$ and $\mathbf{r}'$ are the position vectors of the observation point and source point respectively. also,

$$G(\mathbf{r},\mathbf{r}') = \frac{e^{-j\beta R}}{4\pi R}, \tag{6}$$

$$R = |\mathbf{r} - \mathbf{r}'|. \tag{7}$$

In Eq. (5), ∇ and ∇' are, respectively, the gradients with respect to the observation and source coordinates and $G(\mathbf{r},\mathbf{r}')$ is referred to as Green's function for a three-dimensional scatterer.

If the observations are restricted on the surface of the scatterer ($\mathbf{r} = \mathbf{r}_s$), then Eq. (5) through Eq. (7) can be expressed using Eq. (2)

as

$$j\frac{\eta}{\beta}\left[\beta^2\iint_S \mathbf{J}_s(\mathbf{r}')G(\mathbf{r}_s,\mathbf{r}')ds'+\nabla\iint_S \nabla'\cdot\mathbf{J}_s(\mathbf{r}')G(\mathbf{r}_s,\mathbf{r}')ds'\right]=\mathbf{E}_t^{\text{inc}}(\mathbf{r}=\mathbf{r}_s). \tag{8}$$

Because the right side of Eq. (8) is expressed in terms of the known incident electric field, it is referred to as the electric field integral equation (EFIE). It can be used to find the current density $\mathbf{J}_s(\mathbf{r}')$ at any point $\mathbf{r}=\mathbf{r}'$ on the scatterer. It should be noted that Eq. (8) is actually an integro-differential equation, but usually it is referred to as an integral equation.

Equation (8) is a general surface EFIE for three-dimensional problems and its form can be simplified for two-dimensional geometries.

3. WAVELET: DEFINITION AND EXPANSION, THE SHANNON SYSTEM

A wavelet is a "small wave", which has its energy concentrated in time to give a tool for the analysis of transient, nonstationary, or time-varying phenomena [59]. It still has the oscillating wave-like characteristic but also has the ability to allow simultaneous time and frequency analysis with a flexible mathematical function.

In this section, the definition of wavelets and expansion of any function $f(t)$ in terms of these basis functions is presented. Also, the Shannon wavelet system is introduced.

3.1. Definition and Expansion

We start by defining the scaling function and then define the wavelet in terms of it.

Let $\mathcal{L}^2(\mathbb{R})$ be the space of square integrable functions. A set of scaling functions in terms of integer translates of the basic scaling function or father wavelet $\varphi(t)$ is defined by [59]

$$\varphi_k(t)=\varphi(t-k), \qquad k\in\mathbb{Z}, \qquad \varphi\in\mathcal{L}^2(\mathbb{R}). \tag{9}$$

The subspace of $\mathcal{L}^2(\mathbb{R})$ spanned by these functions is defined as

$$\mathcal{V}_0=\overline{\underset{k\in\mathbb{Z}}{\text{Span}}\{\varphi_k(t)\}}. \tag{10}$$

This means that

$$f(t)=\sum_k c_k\varphi_k(t) \qquad \text{for any } f(t)\in\mathcal{V}_0. \tag{11}$$

One can generally increase the size of the subspace spanned by changing the time scale of the scaling function. A two-dimensional family of functions is generated from the basic scaling function or father wavelet by scaling and translation by [59]

$$\varphi_{j,k}(t) = 2^{j/2}\varphi(2^j t - k), \tag{12}$$

whose span over k is

$$\mathcal{V}_j = \overline{\underset{k\in\mathbb{Z}}{\text{Span}}\{\varphi_k(2^j t)\}} = \overline{\underset{k\in\mathbb{Z}}{\text{Span}}\{\varphi_{j,k}(t)\}}. \tag{13}$$

So, $\{\varphi_{j,k}(t)\}_k$ is a basis for $\mathcal{V}_j$. This means that if $f(t) \in \mathcal{V}_j$, then it can be expressed as

$$f(t) = \sum_{k\in\mathbb{Z}} c_k \varphi_{j,k}(t), \tag{14}$$

where Eq. (14) represents the projection of the function f onto the subspace of scaling functions or father wavelets at resolution j.

According to the above definitions, it is clear that

$$\mathcal{V}_j \subset \mathcal{V}_{j+1} \qquad \text{for all } j \in \mathbb{Z}. \tag{15}$$

The nesting of the spans of $\varphi(2^j t - k)$, denoted by $\mathcal{V}_j$ and shown in Eq. (15), is achieved by requiring that $\varphi(t) \in \mathcal{V}_1$, which means that if $\varphi(t)$ is in $\mathcal{V}_0$, it is also in $\mathcal{V}_1$, the space spanned by $\varphi(2t)$. This means $\varphi(t)$ can be expressed in terms of a weighted sum of shifted $\varphi(2t)$ as

$$\varphi(t) = \sum_{n\in\mathbb{Z}} h(n)\sqrt{2}\varphi(2t - n), \tag{16}$$

where the sequence $\{h(n)\}$ of real or perhaps complex numbers is called the scaling function or father wavelet coefficients (or the scaling filter or the scaling vector) and the $\sqrt{2}$ maintains the norm of the scaling function with the scale of two.

The Eq. (16) is called the refinement equation, the multiresolution analysis (MRA) equation, or the dilation equation [59, 60]. Now, a different set of functions $\psi_{j,k}(t)$ can be defined that span the differences between the spaces spanned by the various scales of the scaling function. These functions are the mother wavelets. There are several advantages to requiring that the father wavelets and mother wavelets be orthogonal. Orthogonal basis functions allow simple calculation of expansion coefficients satisfying Parseval's theorem that allows a partitioning of the signal energy in the wavelet transform domain. The

orthogonal complement of $\mathcal{V}_j$ in $\mathcal{V}_{j+1}$ is defined as $\mathcal{W}_j$. This means that all members of $\mathcal{V}_j$ are orthogonal to all members of $\mathcal{W}_j$. We require

$$< \varphi_{j,k}(t), \psi_{j,l}(t) >= \int \varphi_{j,k}(t)\psi_{j,l}(t)dt = 0, \tag{17}$$

for all appropriate $j, k, l \in \mathbb{Z}$.

The relationship of the various subspaces can be seen from the following expressions. Using Eq. (15) we may start at any $\mathcal{V}_j$, say at $j = 0$, and write

$$\mathcal{V}_0 \subset \mathcal{V}_1 \subset \mathcal{V}_2 \subset \cdots \subset \mathcal{L}^2(\mathbb{R}). \tag{18}$$

Now, the wavelet spanned subspace $\mathcal{W}_j$ can be defined such that

$$\mathcal{V}_1 = \mathcal{V}_0 \oplus \mathcal{W}_0,$$

which extends to

$$\mathcal{V}_2 = \mathcal{V}_0 \oplus \mathcal{W}_0 \oplus \mathcal{W}_1.$$

In general this gives

$$\mathcal{L}^2 = \mathcal{V}_0 \oplus \mathcal{W}_0 \oplus \mathcal{W}_1 \oplus \ldots, \tag{19}$$

when $\mathcal{V}_0$ is the initial space spanned by the scaling function $\varphi(t - k)$.

The scale of the initial space is arbitrary and could be chosen at a higher resolution of, say, $j = j_0$ to give

$$\mathcal{L}^2 = \mathcal{V}_{j_0} \oplus \mathcal{W}_{j_0} \oplus \mathcal{W}_{j_0+1}, \tag{20}$$

or at even $j = -\infty$ where Eq. (20) becomes

$$\mathcal{L}^2 = \cdots \oplus \mathcal{W}_{-2} \oplus \mathcal{W}_{-1} \oplus \mathcal{W}_0 \oplus \mathcal{W}_1 \oplus \mathcal{W}_2 \ldots \tag{21}$$

Since these mother wavelets reside in the space spanned by the next narrower father wavelet, $\mathcal{W}_0 \subset \mathcal{V}_1$, they can be represented by a weighted sum of shifted father wavelet $\varphi(2t)$ defined in Eq. (16) by

$$\psi(t) = \sum_{n\in\mathbb{Z}} h_1(n)\sqrt{2}\varphi(2t - n), \tag{22}$$

for some sequences of coefficients $\{h_1(n)\}$. It can be shown that the mother wavelet coefficients are required by orthogonality to be related to the father wavelet coefficients by [59, 60]

$$h_1(n) = (-1)^n h(1 - n), \tag{23}$$

the function generated by (22) gives the mother wavelet $\psi(t)$ for a class of expansion functions of the form

$$\psi_{j,k}(t) = 2^{j/2}\psi(2^j t - k), \qquad j,k \in \mathbb{Z}, \tag{24}$$

where 2^j is the scaling of t, $2^{-j}k$ is the translation in t, and $2^{j/2}$ maintains the $\mathcal{L}^2$ norm of the wavelet at different scales.

The set of these functions is a basis for the space of square integrable functions $\mathcal{L}^2(\mathbb{R})$, i.e.,

$$f(t) = \sum_j \sum_k d_{j,k}\psi_{j,k}(t), \qquad f(t) \in \mathcal{L}^2(\mathbb{R}). \tag{25}$$

3.2. The Shannon Wavelet System

Wavelets are grouped into families, with names such as the Haar wavelets, the Mexican Hat wavelets, the Shannon wavelets and etc. [61].

Shannon wavelets are the real part of the so-called harmonic wavelets [62–64]. They have a slow decay in the time domain but a very sharp compact support in the frequency (Fourier) domain. This fact, together with the Parseval's identity is used to easily compute the inner product and the expansion coefficients of the Shannon wavelets [62, 65].

A set of Shannon scaling functions or father wavelets in the subspace $\mathcal{V}_j$ is defined as [65]

$$\varphi_{j,k}(t) = 2^{j/2}\frac{\sin\pi(2^j t - k)}{\pi(2^j t - k)}, \qquad k \in \mathbb{Z}. \tag{26}$$

It is clear that for $j = k = 0$, we have the basic scaling function or father wavelet which is shown in Fig. 1.

The mother wavelets are

$$\psi_{j,k}(t) = 2^{j/2}\frac{\sin\pi\left(2^j t - k - \frac{1}{2}\right) - \sin 2\pi\left(2^j t - k - \frac{1}{2}\right)}{\pi\left(2^j t - k - \frac{1}{2}\right)}, \quad k \in \mathbb{Z}. \tag{27}$$

Fig. 2 shows the basic mother wavelet for $j = k = 0$.

The Fourier transforms of these functions are respectively obtained of the following equations [66]:

$$\widehat{\varphi}_{j,k}(\omega) = \frac{2^{-j/2}}{2\pi}e^{-i\omega k/2^j}\chi\left(\omega/2^j + 3\pi\right), \tag{28}$$

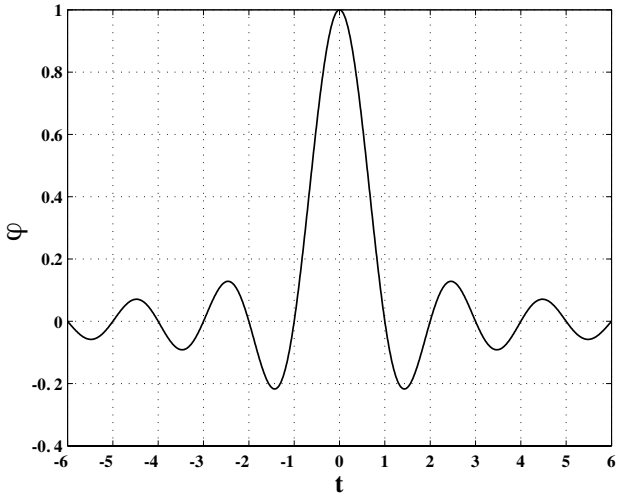

Figure 1. Shannon father wavelet φ as a function of t.

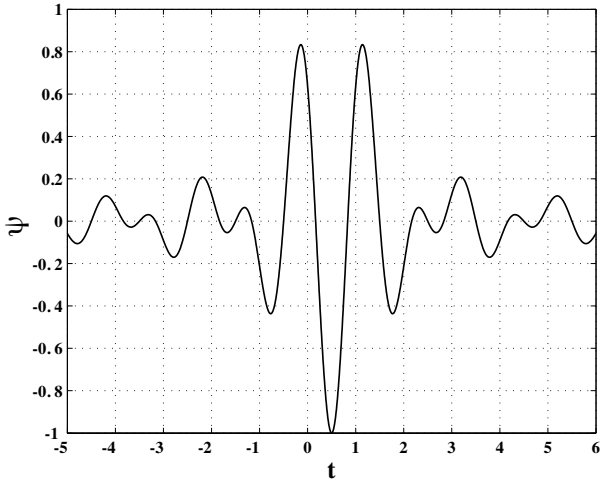

Figure 2. Shannon mother wavelet ψ as a function of t.

and

$$\widehat{\psi}_{j,k}(\omega) = -\frac{2^{-j/2}}{2\pi} e^{-i\omega(k+1/2)/2^j} \left[\chi\left(\omega/2^{j-1}\right) + \chi\left(-\omega/2^{j-1}\right)\right], \quad (29)$$

where, the characteristic function $\chi(\omega)$ is defined as

$$\chi(\omega) = \begin{cases} 1, & 2\pi \leq \omega < 4\pi, \\ 0, & \text{otherwise.} \end{cases} \tag{30}$$

The family of functions $\{\psi_{j,k}(t)\}$ is an orthogonal wavelet basis with respect to the inner product defined as

$$< \psi_{j,k}(t), \psi_{j,l}(t) >= \int_{-\infty}^{\infty} \psi_{j,k}(t)\psi_{j,l}(t)dt, \tag{31}$$

which, according to the Parseval's identity, can be expressed as [66]

$$\begin{aligned} &< \psi_{j,k}(t), \psi_{j,l}(t) >= \int_{-\infty}^{\infty} \psi_{j,k}(t)\psi_{j,l}(t)dt = \\ &2\pi \int_{-\infty}^{\infty} \widehat{\psi}_{j,k}(\omega)\widehat{\psi}^{*}_{j,l}(\omega)d\omega = 2\pi < \widehat{\psi}_{j,k}(\omega), \widehat{\psi}^{*}_{j,l}(\omega) >, \end{aligned} \tag{32}$$

where, '$*$' stands for the complex conjugate.

4. IMPLEMENTING THE METHOD OF MOMENTS USING SHANNON WAVELET BASIS FUNCTIONS

In this section, we apply the Shannon wavelets as orthogonal basis functions in solving the integral equations of the first or second kind by moments method.

Consider the following Fredholm integral equation of the first kind:

$$\int_{a}^{b} k(s,t)x(t)dt = y(s), \tag{33}$$

where, $k(s,t)$ and $y(s)$ are known functions but $x(t)$ is unknown. We can select a sequence of finite dimensional subspaces $\mathcal{V}_j \subset \mathcal{L}^2(\mathbb{R})$, $j \geq 1$. Let $\{\varphi_{n,k}\}_{k=1}^{n}$ be a wavelet basis for $\mathcal{V}_j$ in which, $n = 2^j$. This means that we consider the resolution or scale j. Moreover, $k(s,t) \in \mathcal{L}^2([a,b) \times [a,b))$ and $y(s) \in \mathcal{L}^2([a,b))$. Approximating the function $x(s)$ with respect to the Shannon wavelet basis functions by (14) gives:

$$x(s) \simeq \sum_{k=1}^{n} c_k \varphi_{n,k}(s), \tag{34}$$

such that the c_ks are wavelet coefficients of $x(s)$ that should be determined.

Substituting Eq. (34) into (33) follows:

$$\sum_{k=1}^{n} c_k \int_a^b k(s,t)\varphi_{n,k}(t)dt \simeq y(s). \tag{35}$$

Now, let s_i, $i = 1, 2, \ldots, n$, be n appropriate points in interval $[a, b)$; putting $s = s_i$ in Eq. (35) follows:

$$\sum_{k=1}^{n} c_k \int_a^b k(s_i,t)\varphi_{n,k}(t)dt \simeq y(s_i), \quad i = 1, 2, \ldots, n, \tag{36}$$

or:

$$\sum_{k=1}^{n} \left[c_k \int_a^b k(s_i,t)\varphi_{n,k}(t)dt \right] \simeq y(s_i), \quad i = 1, 2, \ldots, n. \tag{37}$$

Now, replace $\simeq$ with $=$, hence Eq. (37) is a linear system of n algebraic equations for n unknown coefficients $c_1, c_2, \ldots, c_n$. So, an approximate solution $x(s) \simeq \sum_{k=1}^{n} c_k \varphi_{n,k}(s)$, is obtained for Eq. (33).

For a Fredholm integral equation of the second kind, we can rewrite the Eq. (33) as follows:

$$x(s) + \int_a^b k(s,t)x(t)dt = y(s). \tag{38}$$

Using the same procedure mentioned above, we obtain

$$\sum_{k=1}^{n} c_k \left[\varphi_{n,k}(s_i) + \int_a^b k(s_i,t)\varphi_{n,k}(t)dt \right] \simeq y(s_i), \quad i = 1, 2, \ldots, n. \tag{39}$$

Eq. (39) is a linear system of n algebraic equations for n unknown coefficients $c_1, c_2, \ldots, c_n$. So, an approximate solution $x(s) \simeq \sum_{k=1}^{n} c_k \varphi_{n,k}(s)$, is obtained for Eq. (38).

5. EVALUATING THE RADAR CROSS SECTION OF THE CONDUCTING AND RESISTIVE STRIPS

Now, the RCS of conducting and resistive surfaces is evaluated. We consider two cases for implementing our method; a conducting strip and a resistive strip.

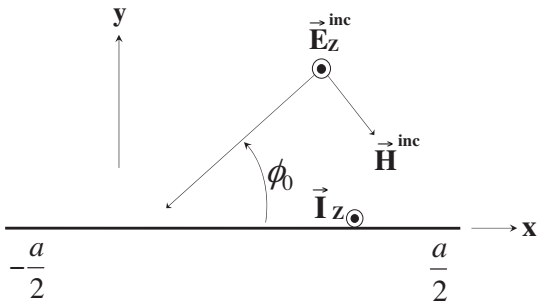

Figure 3. A strip of width a encountered by an incoming TM-polarized plane wave.

In Fig. 3, there is a strip that is very long in the $\pm z$ direction.

Firstly, we assume that we have a conducting strip. The tangential electric field at the surface of a perfect conductor must vanish (i.e., equal zero) [67]. Expressed mathematically:

$$E^{\text{inc}} + E^{\text{scat}} = 0, \tag{40}$$

or

$$E^{\text{inc}} = -E^{\text{scat}}. \tag{41}$$

According to Fig. 3, the incoming electromagnetic wave is polarized with an electric field parallel to the z-axis. This polarization therefore produces a current on the strip that follows along the z-axis. The magnetic field of this wave is entirely in the x-y plane, and is therefore transverse to the z-axis. It is referred as a transverse magnetic (TM) polarized wave.

The magnetic vector potential of the current flowing along the strip is given by [67]

$$A_z = \frac{\mu_0}{4j} \int_{-a/2}^{a/2} I_z(x') H_0^{(2)}(k|x - x'|) dx', \tag{42}$$

where:

$\mu_0 = 4\pi \times 10^{-7}$ H/m, is free space permeability;

$G(x, x') = \frac{1}{4j} H_0^{(2)}(k|x - x'|)$, is 2D free space Green's function;

$H_0^{(2)}(x)$, is a Hankel function of the second kind of zero order.

So, the electric field is given by

$$E_z(x) = j\omega A_z(x), \tag{43}$$

or

$$E(x) = \frac{\omega\mu_0}{4}\int_{-a/2}^{a/2} I_z(x')H_0^{(2)}(k|x-x'|)dx', \tag{44}$$

where, ω is the frequency of the wave.

According to boundary condition (41), the Eq. (44) becomes

$$\int_{-a/2}^{a/2} I_z(x')H_0^{(2)}(k|x-x'|)dx' = -\frac{4}{\omega\mu_0}E^{\text{inc}}(x). \tag{45}$$

Choosing $E^{\text{inc}}(x) = e^{jkx\cos\phi_0}$:

$$\int_{-a/2}^{a/2} I_z(x')H_0^{(2)}(k|x-x'|)dx' = -\frac{4}{\omega\mu_0}e^{jkx\cos\phi_0}. \tag{46}$$

It is a Fredholm integral equation of the first kind with complex kernel of the following form:

$$\int_a^b G(x,x')h(x')dx' = g(x), \tag{47}$$

where:
$h(x) = I_z(x)$;
$G(x,x') = H_0^{(2)}(k|x-x'|)$;
$g(x) = -\frac{4}{\omega\mu_0}e^{jkx\cos\phi_0}$.

Now, consider a resistive strip and assume that $R_s(x)$ is its surface resistance. Note that the units of surface resistance are in Ω/m^2. The boundary condition at the surface of a thin resistive strip is given by the following equation [67]:

$$-E^{\text{inc}} = E^{\text{scat}} + R_s(x)I_z(x), \tag{48}$$

where, $I_z(x)$ is the surface current of the strip. Assuming $E^{\text{inc}} = e^{jkx\cos\phi_0}$, from Eq. (44) and Eq. (48) it follows:

$$R_s(x)I_z(x) + \frac{\omega\mu_0}{4}\int_{-a/2}^{a/2} I_z(x')H_0^{(2)}(k|x-x'|)dx' = -e^{jkx\cos\phi_0}. \tag{49}$$

Eq. (49) can be converted to the following equation:

$$h(x) + \int_a^b G(x, x')h(x')dx' = g(x), \tag{50}$$

where:

$h(x) = I_z(x)$;
$G(x, x') = \frac{\omega\mu_0}{4}\frac{1}{R_s(x)}H_0^{(2)}(k|x - x'|)$;
$g(x) = -\frac{1}{R_s(x)}e^{jkx\cos\phi_0}$.

This is a Fredholm integral equation of the second kind and can be solved by the presented method. However, from Eqs. (46) and (49) $I_z(x)$ can be obtained and then the RCS of the strip can be computed easily.

The radar cross section in two dimensions is defined mathematically as [67]

$$\sigma(\phi) = \lim_{r\to\infty} 2\pi r\frac{|\mathbf{E}^{\text{scat}}|^2}{|\mathbf{E}^{\text{inc}}|^2}. \tag{51}$$

In the presented case, the RCS is obtained of the following equation [67]:

$$\sigma(\phi) = \frac{k\eta^2}{4}\left|\int_{-a/2}^{a/2} I_z(x')e^{jkx'\cos\phi}dx'\right|^2. \tag{52}$$

Also, it is possible to define a logarithmic quantity with respect to the RCS, so that

$$\sigma_{\text{dBlm}} = 10\log_{10}\ \sigma. \tag{53}$$

Although we can now calculate the current distribution and RCS using our proposed method, but we prefer to check the validity and accuracy of this approach on some examples firstly, and then deal with the main problem.

5.1. Numerical Examples

Here, we solve some integral equations to show the accuracy of presented method. Also, we compare our obtained results with the results that we have calculated via implementing the moments method using the well-known BPFs. It should be mentioned that the integral

equations have been selected such that their kernels and the kernel of Eqs. (46) and (49) are identical (i.e., Hankel function). Also, we remind the reader that an m-set of block-pulse functions over any interval $[a, b)$ is defined as [58]

$$P_i(t) = \begin{cases} 1, & a + i(b-a)/n \le t < a + (i+1)(b-a)/n, \\ 0, & \text{otherwise}, \end{cases} \tag{54}$$

where, $i = 0, 1, \ldots, n-1$, with a positive integer value for n.

Example 1. Consider the following Fredholm integral equation of the first kind:

$$\int_{-a/2}^{a/2} G(x, x')I(x') = f(x), \tag{55}$$

with the exact solution $I(x) = \ln(x + a) + ix$, and suitable right hand side $[f(x)]$ which can be obtained of numerical integration. Also, $G(x, x') = H_0^{(2)}(k|x - x'|)$ and $i = \sqrt{-1}$. Solving this equation via presented method gives the approximate solution of $I(x)$. The exact and approximate values of $I(x)$ magnitude for $a = 0.5$, $k = 2\pi$, and for scale $j = 2$ ($n = 4$) have been calculated at nine specific points and shown in Table 1. Note that "MM" means "Moments Method".

Table 1. Numerical results for example 1 ($n = 4$).

x	Exact solution	MM using Shannon wavelets	MM using BPFs
−0.20	1.2205	1.2196	1.2047
−0.15	1.0605	1.1072	1.2047
−0.10	0.9217	0.9467	0.8252
−0.05	0.8001	0.7874	0.8252
0.00	0.6931	0.6649	0.0000
0.05	0.5999	0.5892	0.5756
0.10	0.5205	0.5430	0.5756
0.15	0.4562	0.4924	0.4081
0.20	0.4089	0.4090	0.4081

Example 2. Assume that the Eq. (55) has the exact solution $I(x) = x\ln(x + a) + i\sin(4x^2/a^2)$. The exact and approximate values of $I(x)$ magnitude for $a = 0.5$, $k = 2\pi$, and for scale $j = 3$ ($n = 8$) are shown in Table 2.

Table 2. Numerical results for example 2 ($n = 8$).

x	Exact solution	MM using Shannon wavelets	MM using BPFs
−0.20	0.6439	0.6386	0.7642
−0.15	0.3859	0.3775	0.4138
−0.10	0.1838	0.1862	0.1598
−0.05	0.0565	0.0609	0.0260
0.00	0.0000	0.0018	0.0000
0.05	0.0499	0.0471	0.0224
0.10	0.1673	0.1648	0.1443
0.15	0.3582	0.3599	0.3846
0.20	0.6014	0.6112	0.7128

Example 3. As the final example, consider the following Fredholm integral equation of the second kind:

$$I(x) + \int_{-a/2}^{a/2} G(x, x')I(x') = f(x), \tag{56}$$

with the exact solution $I(x) = \left(x^4 - \exp(-x^2/a^2)\right)\sin^2(x/a^2)$, and suitable right hand side $[f(x)]$. Also, $G(x, x') = H_0^{(2)}(k|x - x'|)$. For $a = 0.25$, $k = \pi$, and for scale $j = 3$ ($n = 8$), Table 3 gives the exact and approximate values of $I(x)$ magnitude.

Referring to the numerical results presented in Tables 1–3, it is concluded that the proposed method as a numerical approach has a high accuracy and efficiency for solving integral equations of the form (55) or (56), in which, $G(x, x') = H_0^{(2)}(k|x-x'|)$. Also, the results show that using the Shannon wavelets to implement the moments method for solving these problems leads to higher accuracy than BPFs.

The results presented here have been calculated for $n = 4$ and 8, because for these values of n, the differences between the results of our method and the results obtained of "MM" using BPFs could be more obvious. However, we implemented the method for $n = 16, 32, 64$ and 128 too, and the results approached the exact values, quickly; so that for $n = 16$ and $n = 32$, the mean-absolute errors were around 10^{-4} and 10^{-5}, respectively; and these errors decreased by increasing n. This can confirm good stability and quick convergence of the proposed

Table 3. Numerical results for example 3 ($n = 8$).

x	Exact solution	MM using Shannon wavelets	MM using BPFs
−0.12	0.7011	0.7231	0.7986
−0.09	0.8634	0.8604	0.8159
−0.06	0.6335	0.6341	0.4477
−0.03	0.2102	0.2094	0.0600
0.00	0.0000	0.0001	0.0000
0.03	0.2102	0.2094	0.0600
0.06	0.6335	0.6341	0.4477
0.09	0.8634	0.8604	0.8159
0.12	0.7011	0.7231	0.7986

method. We remind that the mean-absolute error is defined as

$$E_n = \frac{1}{n}\sum_{i=1}^{n} |x(s_i) - x_n(s_i)|\,, \tag{57}$$

where, $x(s)$ is the exact solution and $x_n(s)$ is the approximate solution.

5.2. Calculating the Current Distribution and RCS Via Presented Approach

Now, we have the necessary tools for solving Eqs. (46) and (49). Applying the proposed method in solving these equations gives the current distribution across the conducting or resistive strip, respectively. Then, the RCS can be obtained of Eqs. (52) and (53).

Firstly, assume that the strip is perfect conductor. So, the Eq. (46) should be solved. In Figs. 4–6, the approximate solutions of this equation for $a = \frac{\lambda}{2}$ and $\phi_0 = 0,\ \frac{\pi}{4},\ \frac{\pi}{2}$, and $f = 0.3\,\mathrm{GHz}$ are given. Also, the current distributions for $a = 2\lambda$ and $a = 4\lambda$ are shown in Figs. 7–9 and 10–12, respectively. We have considered scale $j = 5$ ($n = 32$) to obtain these solutions. Considering $\phi_0 = \frac{\pi}{2}$, the bistatic radar cross sections of the strip for $a = 2\lambda, 6\lambda$, and 8λ are respectively given in Figs. 13–15.

Now, consider a resistive strip and assume that the $R_s(x)$ has a uniform distribution throughout the surface of strip. Considering Eq. (49), $I(x)$ is computed for R_s of 500 and $1000\,(\Omega/\mathrm{m}^2)$, $\phi_0 = \frac{\pi}{2}$, $a = 6\lambda$, $f = 0.3\,\mathrm{GHz}$, and $j = 4$ ($n = 16$); and then RCS is obtained of

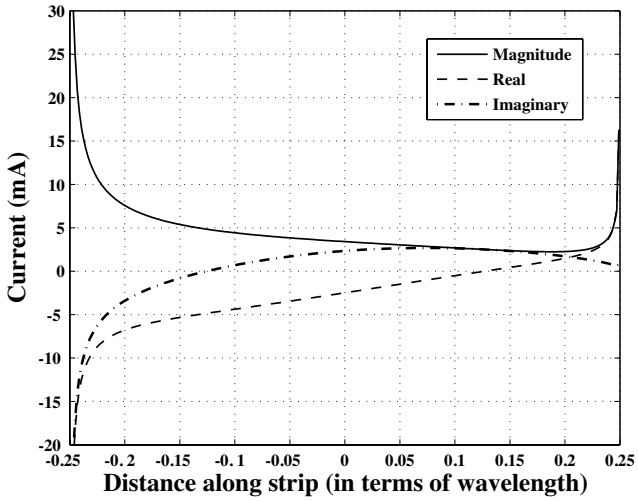

Figure 4. Current distribution across a $\frac{\lambda}{2}$-wide conducting strip created by a TM-polarized plane wave for $\phi_0 = 0$, and $n = 32$.

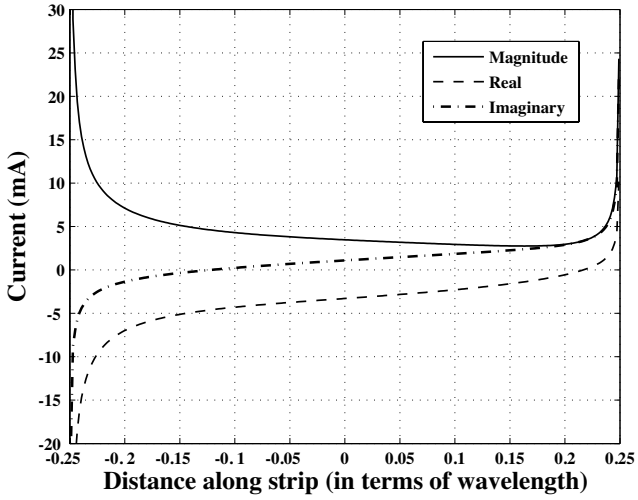

Figure 5. Current distribution across the $\frac{\lambda}{2}$-wide conducting strip for $\phi_0 = \frac{\pi}{4}$, and $n = 32$.

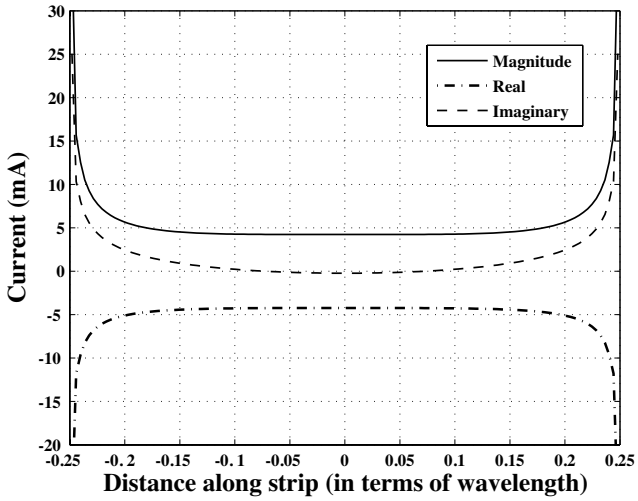

Figure 6. Current distribution across the $\frac{\lambda}{2}$-wide conducting strip for $\phi_0 = \frac{\pi}{2}$, and $n = 32$.

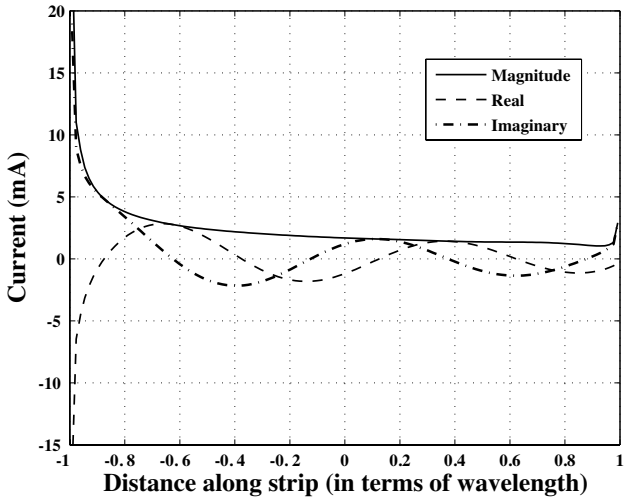

Figure 7. Current distribution across a 2λ-wide conducting strip created by a TM-polarized plane wave for $\phi_0 = 0$, and $n = 32$.

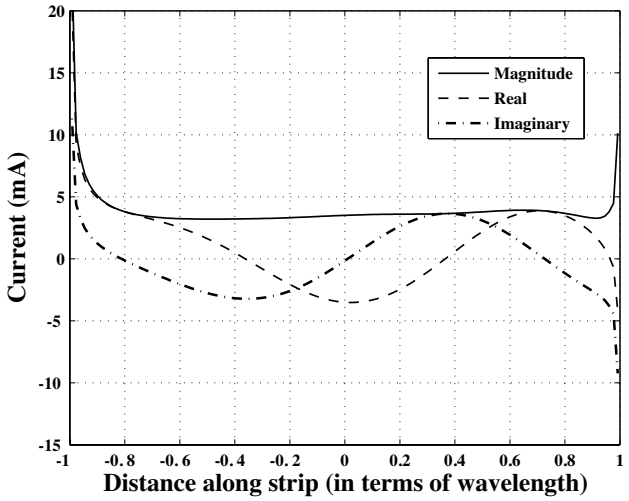

Figure 8. Current distribution across the 2λ-wide conducting strip for $\phi_0 = \frac{\pi}{4}$, and $n = 32$.

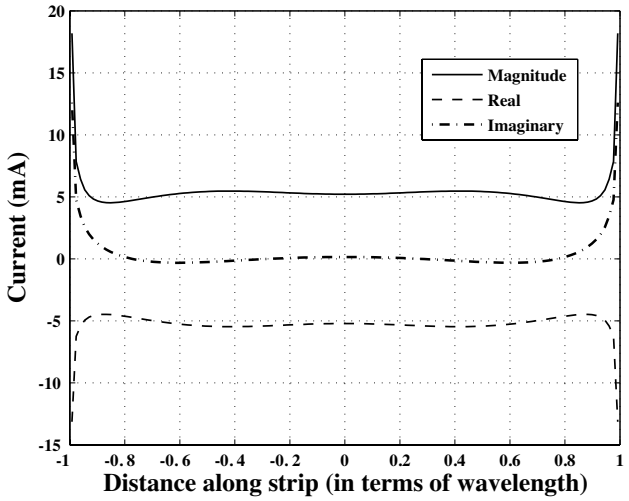

Figure 9. Current distribution across the 2λ-wide conducting strip for $\phi_0 = \frac{\pi}{2}$, and $n = 32$.

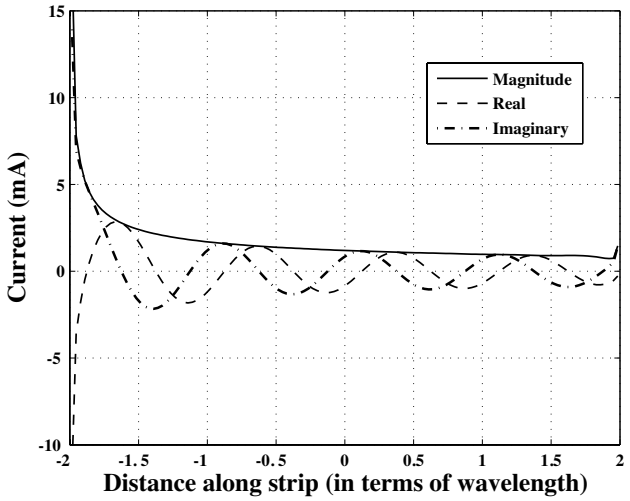

Figure 10. Current distribution across a 4λ-wide conducting strip created by a TM-polarized plane wave for $\phi_0 = 0$, and $n = 32$.

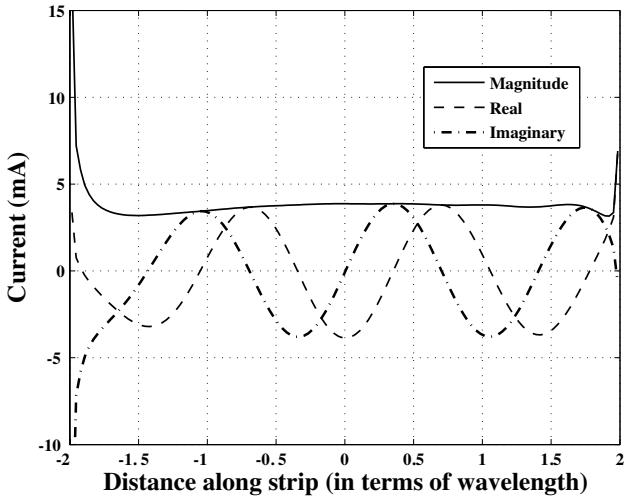

Figure 11. Current distribution across the 4λ-wide conducting strip for $\phi_0 = \frac{\pi}{4}$, and $n = 32$.

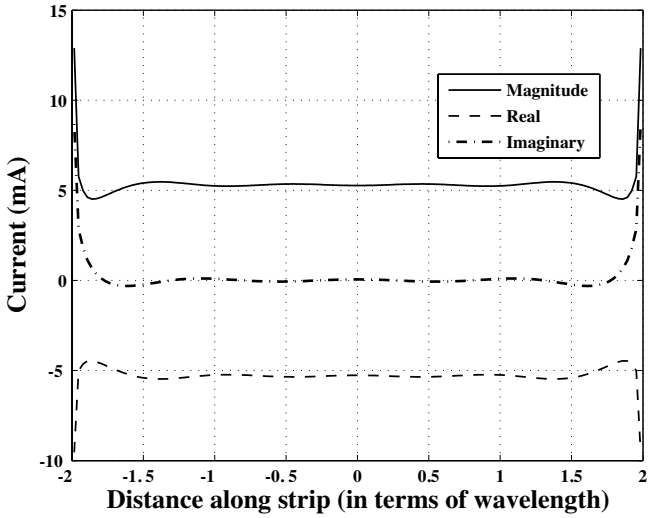

Figure 12. Current distribution across the 4λ-wide conducting strip for $\phi_0 = \frac{\pi}{2}$, and $n = 32$.

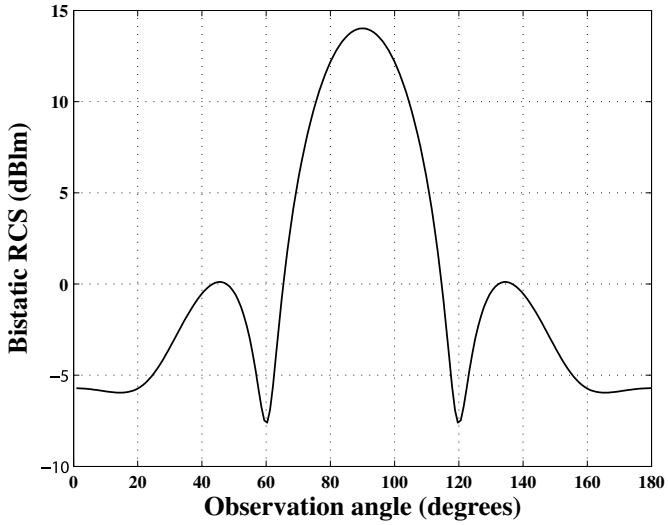

Figure 13. The bistatic RCS of a 2λ-wide conducting strip for $\phi_0 = \frac{\pi}{2}$.

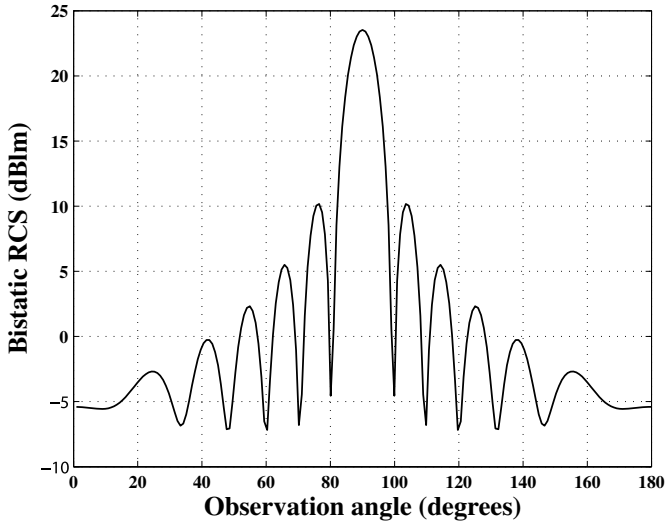

Figure 14. The bistatic RCS of a 6λ-wide conducting strip for $\phi_0 = \frac{\pi}{2}$.

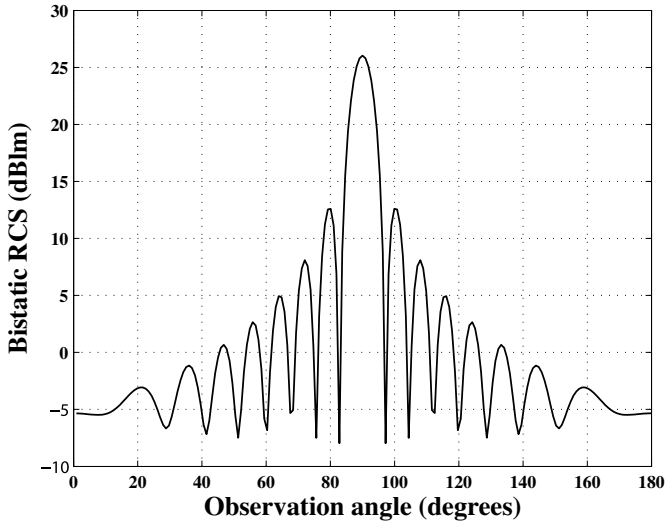

Figure 15. The bistatic RCS of a 8λ-wide conducting strip for $\phi_0 = \frac{\pi}{2}$.

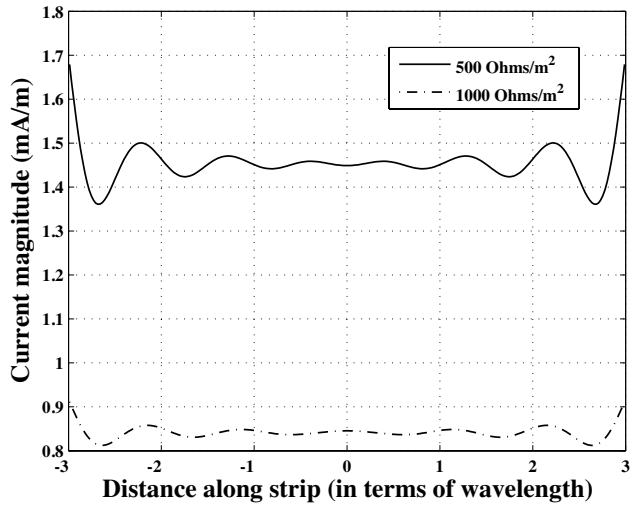

Figure 16. Current magnitude across a 6λ-wide resistive strip for R_s of 500 and 1000 (Ω/m^2), $\phi_0 = \frac{\pi}{2}$, and $n = 16$.

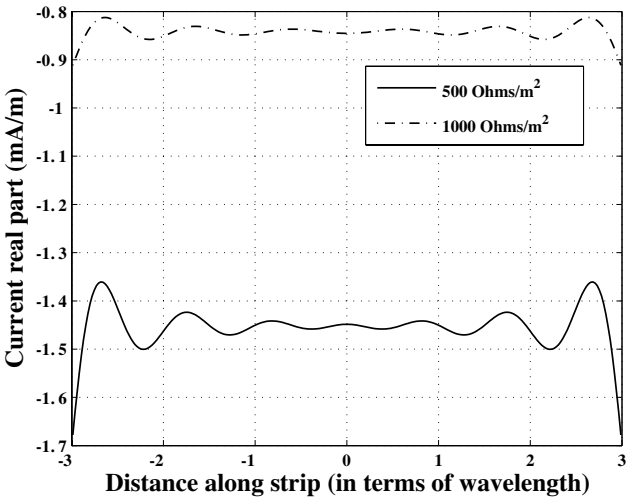

Figure 17. The real part of current across the 6λ-wide resistive strip for R_s of 500 and 1000 (Ω/m^2), $\phi_0 = \frac{\pi}{2}$, and $n = 16$.

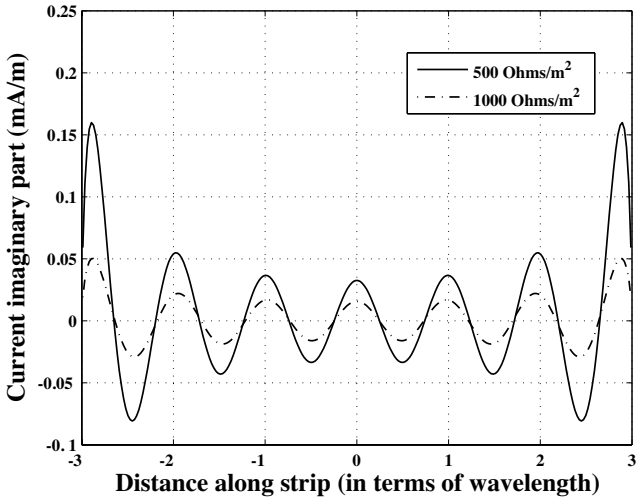

Figure 18. The imaginary part of current across the 6λ-wide resistive strip for R_s of 500 and 1000 (Ω/m^2), $\phi_0 = \frac{\pi}{2}$, and $n = 16$.

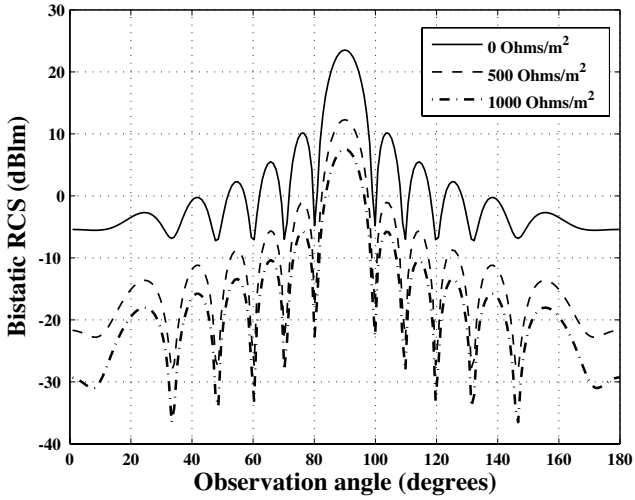

Figure 19. The bistatic RCS of the 6λ-wide resistive strip for R_s of 0, 500, 1000 (Ω/m^2), and $\phi_0 = \frac{\pi}{2}$.

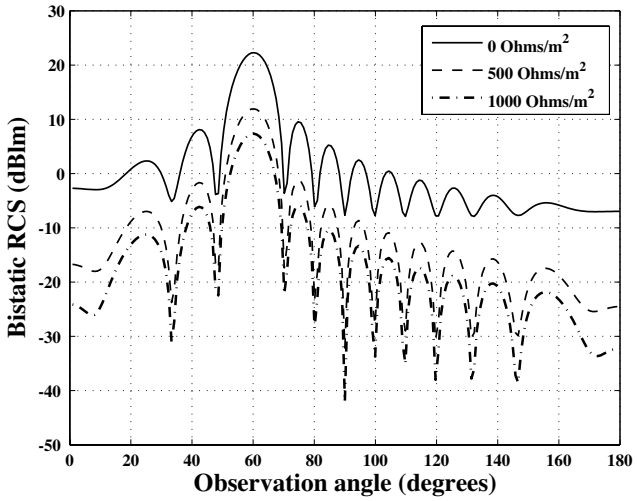

Figure 20. The bistatic RCS of the 6λ-wide resistive strip for R_s of 0, 500, 1000 (Ω/m^2), and $\phi_0 = \frac{2\pi}{3}$.

Eqs. (52) and (53). The current distributions of the resistive strip for these values of R_s are shown in Figs. 16–18. Figs. 19 and 20 give the bistatic RCS of the 6λ-wide resistive strip, for R_s of 0, 500, 1000 (Ω/m^2), and for $\phi_0 = \frac{\pi}{2},\ \frac{2\pi}{3}$. Also, in Fig. 21 the monostatic RCS of this strip is given. It is seen that the level of the first side lobe is nearly 13 dB down from the main lobe.

Finally, consider a quadratic resistive taper expressed by

$$R_s(x) = 2\eta \left(\frac{kx}{a}\right)^2 \qquad (\Omega/\mathrm{m}^2), \tag{58}$$

where, k is a real coefficient.

Figure 22 shows the quadratic taper of a 6λ-wide strip for $k = 2$. After computing $I(x)$ by Eq. (49), the RCS of this strip can be obtained. For $\phi_o = \frac{\pi}{2}$ and $j = 6$ $(n = 64)$, the magnitude, real part and imaginary part of strip current are shown in Figs. 23 and 24, and the bistatic radar cross section of this strip shown in Figs. 25 and 26 has been calculated for $k = 0.5,\ 1,\ 2$, $\phi_0 = \frac{\pi}{2},\ \frac{\pi}{4}$, and $f = 0.3$ GHz. Fig. 27 shows the monostatic RCS. It is seen that the quadratic taper reduces the first side lobe to a level of -23 dB below the main lobe. This taper has reduced the first side lobe by 10 dB, compared with a uniform distribution.

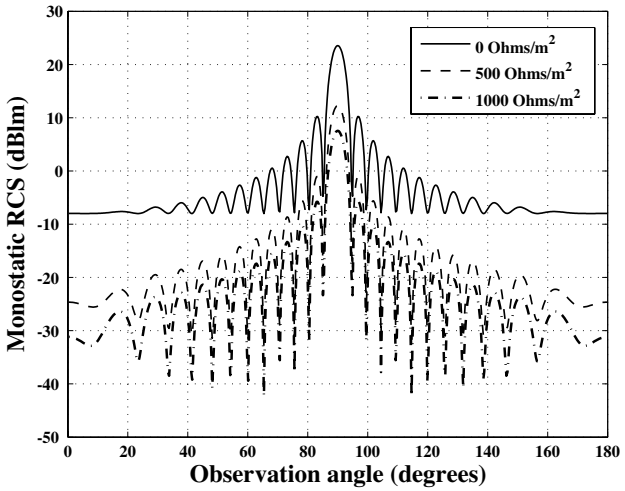

Figure 21. The monostatic RCS of the 6λ-wide resistive strip for R_s of 0, 500, 1000 (Ω/m^2).

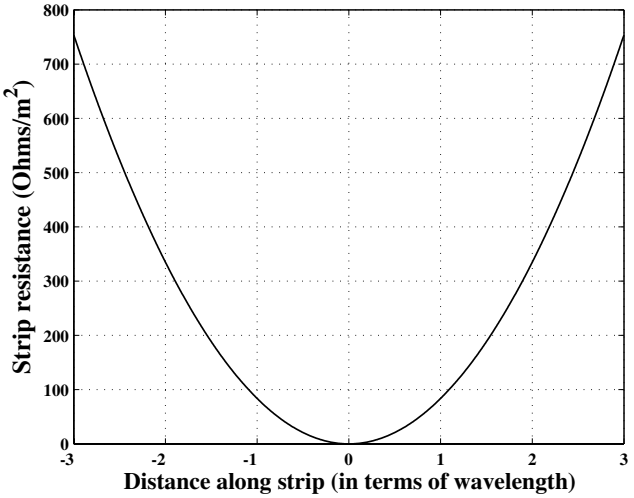

Figure 22. The quadratic taper of a 6λ-wide resistive strip for $k = 2$.

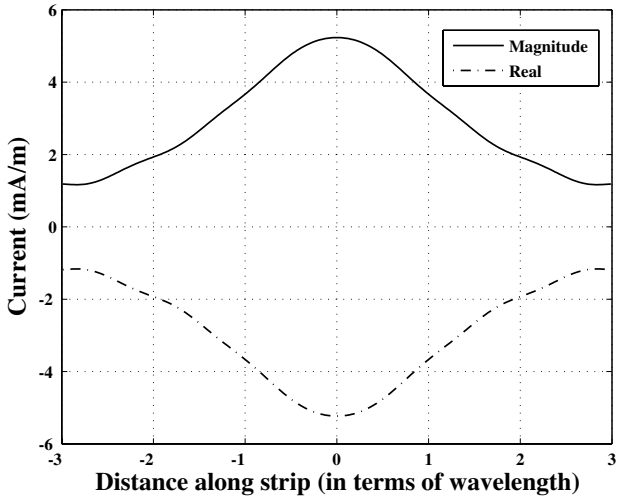

Figure 23. The magnitude and real part of current across the 6λ-wide resistive strip of Fig. 22 for $k = 2$, $f = 0.3\,\mathrm{GHz}$, and $n = 64$.

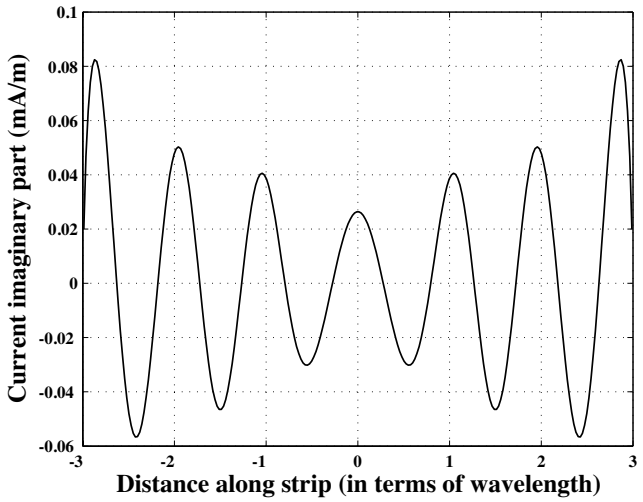

Figure 24. The imaginary part of current across the 6λ-wide resistive strip of Fig. 22 for $k = 2$, $f = 0.3\,\mathrm{GHz}$, and $n = 64$.

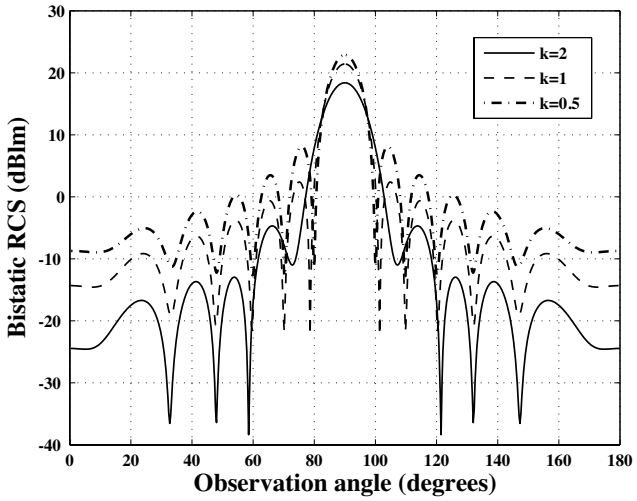

Figure 25. The bistatic RCS of the 6λ-wide resistive strip of Fig. 22 for $k = 0.5,\ 1,\ 2$, and $\phi_0 = \frac{\pi}{2}$.

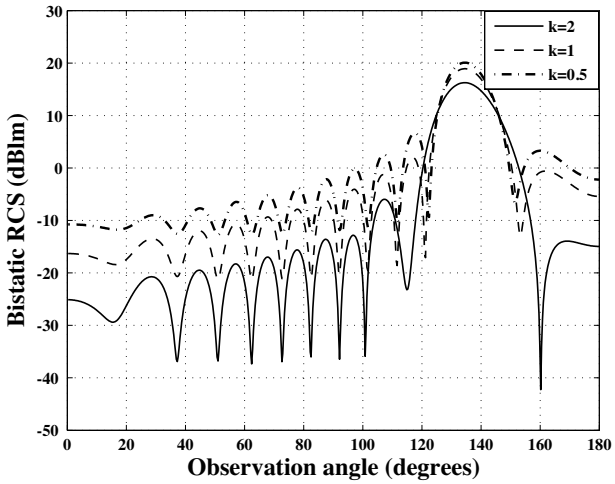

Figure 26. The bistatic RCS of the 6λ-wide resistive strip of Fig. 22 for $k = 0.5,\ 1,\ 2$, and $\phi_0 = \frac{\pi}{4}$.

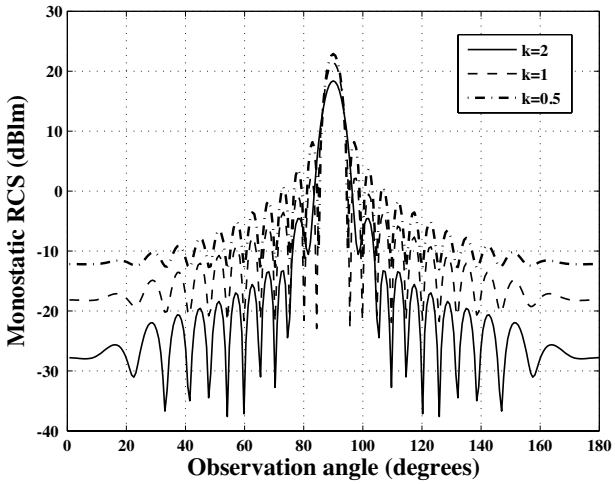

Figure 27. The monostatic RCS of the 6λ-wide resistive strip of Fig. 22 for $k = 0.5,\ 1,\ 2$.

6. CONCLUSION

We proposed a numerical method for evaluating the RCS of conducting and resistive surfaces based on using Shannon wavelet basis functions in moments method.

As the numerical results showed, this method reduces an integral equation of the first or second kind to a linear system of algebraic equations.

The validity and accuracy of this approach was checked on some examples, and the Shannon wavelets were compared with the well-known BPFs from the viewpoint of computational efficiency. The obtained results showed that our method is more accurate.

The problem of RCS was described in detail, and illustrative computations were given for some cases. The presented approach can be generalized to apply to objects of arbitrary geometry and arbitrary material.

REFERENCES

1. Wilton, D. R. and C. M. Butler, "Effective methods for solving integral and integro-differential equations," *Electromagnetics*, Vol. 1, 289–308, 1981.

2. Harrington, R. F., "Matrix methods for field problems," *Proc. IEEE*, Vol. 55, No. 2, 136–149, 1967.
3. Mishra, M. and N. Gupta, "Monte Carlo integration technique for the analysis of electromagnetic scattering from conducting surfaces," *Progress In Electromagnetics Research*, PIER 79, 91–106, 2008.
4. Arnold, M. D., "An efficient solution for scattering by a perfectly conducting strip grating," *Journal of Electromagnetic Waves and Applications*, Vol. 20, No. 7, 891–900, 2006.
5. Zhao, J. X., "Numerical and analytical formulations of the extended MIE theory for solving the sphere scattering problem," *Journal of Electromagnetic Waves and Applications*, Vol. 20, No. 7, 967–983, 2006.
6. Ruppin, R., "Scattering of electromagnetic radiation by a perfect electromagnetic conductor sphere," *Journal of Electromagnetic Waves and Applications*, Vol. 20, No. 12, 1569–1576, 2006.
7. Ruppin, R., "Scattering of electromagnetic radiation by a perfect electromagnetic conductor cylinder," *Journal of Electromagnetic Waves and Applications*, Vol. 20, No. 13, 1853–1860, 2006.
8. Hussein, K. F. A., "Efficient near-field computation for radiation and scattering from conducting surfaces of arbitrary shape," *Progress In Electromagnetics Research*, PIER 69, 267–285, 2007.
9. Hussein, K. F. A., "Fast computational algorithm for EFIE applied to arbitrarily-shaped conducting surfaces," *Progress In Electromagnetics Research*, PIER 68, 339–357, 2007.
10. Kishk, A. A., "Electromagnetic scattering from composite objects using a mixture of exact and impedance boundary conditions," *IEEE Transactions on Antennas and Propagation*, Vol. 39, No. 6, 826–833, 1991.
11. Caorsi, S., A. Massa, and M. Pastorino, "A numerical solution to full-vector electromagnetic scattering by three-dimensional nonlinear bounded dielectrics," *IEEE Transactions on Microwave Theory and Techniques*, Vol. 43, No. 2, 428–436, 1995.
12. Shore, R. A. and A. D. Yaghjian, "Dual-surface integral equations in electromagnetic scattering," *IEEE Transactions on Antennas and Propagation*, Vol. 53, No. 5, 1706–1709, 2005.
13. Ylä-Oijala, P. and M. Taskinen, "Well-conditioned Müller formulation for electromagnetic scattering by dielectric objects," *IEEE Transactions on Antennas and Propagation*, Vol. 53, No. 10, 3316–3323, 2005.
14. Li, L. W., P. S. Kooi, Y. L. Qin, T. S. Yeo, and M. S. Leong,

"Analysis of electromagnetic scattering of conducting circular disk using a hybrid method," *Progress In Electromagnetics Research*, PIER 20, 101–123, 1998.

15. Liu, Y. and K. J. Webb, "On detection of the interior resonance errors of surface integral boundary conditions for electromagnetic scattering problems," *IEEE Transactions on Antennas and Propagation*, Vol. 49, No. 6, 939–943, 2001.
16. Kishk, A. A., "Electromagnetic scattering from transversely corrugated cylindrical structures using the asymptotic corrugated boundary conditions," *IEEE Transactions on Antennas and Propagation*, Vol. 52, No. 11, 3104–3108, 2004.
17. Tong, M. S. and W. C. Chew, "Nyström method with edge condition for electromagnetic scattering by 2d open structures," *Progress In Electromagnetics Research*, PIER 62, 49–68, 2006.
18. Valagiannopoulos, C. A., "Closed-form solution to the scattering of a skew strip field by metallic pin in a slab," *Progress In Electromagnetics Research*, PIER 79, 1–21, 2008.
19. Frangos, P. V. and D. L. Jaggard, "Analytical and numerical solution to the two-potential Zakharov-Shabat inverse scattering problem," *IEEE Transactions on Antennas and Propagation*, Vol. 40, No. 4, 399–404, 1992.
20. Barkeshli, K. and J. L. Volakis, "Electromagnetic scattering from thin strips-Part II: Numerical solution for strips of arbitrary size," *IEEE Transactions on Education*, Vol. 47, No. 1, 107–113, 2004.
21. Collino, F., F. Millot, and S. Pernet, "Boundary-integral methods for iterative solution of scattering problems with variable impedance surface condition," *Progress In Electromagnetics Research*, PIER 80, 1–28, 2008.
22. Zahedi, M. M. and M. S. Abrishamian, "Scattering from semi-elliptic channel loaded with impedance elliptical cylinder," *Progress In Electromagnetics Research*, PIER 79, 47–58, 2008.
23. Zaki, K. A. and A. R. Neureuther, "Scattering from a perfectly conducting surface with a sinusoidal height profile: TE polarization," *IEEE Transactions on Antennas and Propagation*, Vol. 19, No. 2, 208–214, 1971.
24. Carpentiery, B., "Fast iterative solution methods in electromagnetic scattering," *Progress In Electromagnetics Research*, PIER 79, 151–178, 2008.
25. Du, Y., Y. L. Luo, W. Z. Yan, and J. A. Kong, "An electromagnetic scattering model for soybean canopy," *Progress In Electromagnetics Research*, PIER 79, 209–223, 2008.

26. Umashankar, K. R., S. Nimmagadda, and A. Taflove, "Numerical analysis of electromagnetic scattering by electrically large objects using spatial decomposition technique," *IEEE Transactions on Antennas and Propagation*, Vol. 40, No. 8, 867–877, 1992.
27. Gokten, M., A. Z. Elsherbeni, and E. Arvas, "Electromagnetic scattering analysis using the two-dimensional MRFD formulation," *Progress In Electromagnetics Research*, PIER 79, 387–399, 2008.
28. Hatamzadeh-Varmazyar, S., M. Naser-Moghadasi, E. Babolian, and Z. Masouri, "Calculating the radar cross section of the resistive targets using the Haar wavelets," *Progress In Electromagnetics Research*, PIER 83, 55–80, 2008.
29. Hatamzadeh-Varmazyar, S., M. Naser-Moghadasi, E. Babolian, and Z. Masouri, "Numerical approach to survey the problem of electromagnetic scattering from resistive strips based on using a set of orthogonal basis functions," *Progress In Electromagnetics Research*, PIER 81, 393–412, 2008.
30. Hatamzadeh-Varmazyar, S., M. Naser-Moghadasi, and Z. Masouri, "A moment method simulation of electromagnetic scattering from conducting bodies," *Progress In Electromagnetics Research*, PIER 81, 99–119, 2008.
31. Hatamzadeh-Varmazyar, S. and M. Naser-Moghadasi, "New numerical method for determining the scattered electromagnetic fields from thin wires," *Progress In Electromagnetics Research B*, Vol. 3, 207–218, 2008.
32. Hatamzadeh-Varmazyar, S. and M. Naser-Moghadasi, "An integral equation modeling of electromagnetic scattering from the surfaces of arbitrary resistance distribution," *Progress In Electromagnetics Research B*, Vol. 3, 157–172, 2008.
33. Babolian, E., Z. Masouri, and S. Hatamzadeh-Varmazyar, "New direct method to solve nonlinear Volterra-Fredholm integral and integro-differential equations using operational matrix with block-pulse functions," *Progress In Electromagnetics Research B*, Vol. 8, 59–76, 2008.
34. Abd-El-Ranouf, H. E. and R. Mittra, "Scattering analysis of dielectric coated cones," *Journal of Electromagnetic Waves and Applications*, Vol. 21, No. 13, 1857–1871, 2007.
35. Choi, S. and N.-H. Myung, "Scattering analysis of open-ended cavity with inner object," *Journal of Electromagnetic Waves and Applications*, Vol. 21, No. 12, 1689–1702, 2007.
36. Li, Y.-L., J.-Y. Huang, and S.-H. Gong, "The scattering cross section for a target irradiated by time-varying electromagnetic

waves," *Journal of Electromagnetic Waves and Applications*, Vol. 21, No. 9, 1265–1271, 2007.

37. Rui, P.-L. and R. Chen, "Implicity restarted gmres fast Fourier transform method for electromagnetic scattering," *Journal of Electromagnetic Waves and Applications*, Vol. 21, No. 7, 973–976, 2007.
38. Nicolic, N., J. S. Kot, and S. S. Vinogradov, "Scattering by a luneberg lens partially covered by a metallic cap," *Journal of Electromagnetic Waves and Applications*, Vol. 21, No. 4, 549–563, 2007.
39. Yuan, H.-W., S.-X. Gong, X. Wang, and W.-T. Wang, "Scattering analysis of a printed dipole antenna using PBG structures," *Progress In Electromagnetics Research B*, Vol. 1, 189–195, 2008.
40. Faghihi, F. and H. Heydari, "A combination of time domain finite element-boundary integral and with time domain physical optics for calculation of electromagnetic scattering of 3-D structures," *Progress In Electromagnetics Research*, PIER 79, 463–474, 2008.
41. Ahmed, S. and Q. A. Naqavi, "Electromagnetic scattering from a perfect electromagnetic conductor cylinder buried in a dielectric half-space," *Progress In Electromagnetics Research*, PIER 78, 25–38, 2008.
42. Valagiannopoulos, C. A., "Electromagnetic scattering from two eccentric metamaterial cylinders with frequency-dependent permittivities differing slightly each other," *Progress In Electromagnetics Research B*, Vol. 3, 23–34, 2008.
43. Hady, L. K. and A. A. Kishk, "Electromagnetic scattering from conducting circular cylinder coated by meta-materials and loaded with helical strips under oblique incidence," *Progress In Electromagnetics Research B*, Vol. 3, 189–206, 2008.
44. Zainud-Deen, S. H., A. Z. Botros, and M. S. Ibrahim, "Scattering from bodies coated with metamaterial using FDFD method," *Progress In Electromagnetics Research B*, Vol. 2, 279–290, 2008.
45. Li, Y.-L., J.-Y. Huang, M.-J. Wang, and J. Zhang, "Scattering field for the ellipsoidal targets irradiated by an electromagnetic wave with arbitrary polarizing and propagating direction," *Progress In Electromagnetics Research Letters*, Vol. 1, 221–235, 2008.
46. Xu, L., Y.-C. Guo, and X.-W. Shi, "Dielectric half space model for the analysis of scattering from objects on ocean surface," *Journal of Electromagnetic Waves and Applications*, Vol. 21, No. 15, 2287–2296, 2007.

47. Zhong, X. J., T. Cui, Z. Li, Y.-B. Tao, and H. Lin, "Terahertz-wave scattering by perfectly electrical conducting objects," *Journal of Electromagnetic Waves and Applications*, Vol. 21, No. 15, 2331–2340, 2007.
48. Li, Y.-L., J.-Y. Huang, and M.-J. Wang, "Scattering cross section for airborne and its application," *Journal of Electromagnetic Waves and Applications*, Vol. 21, No. 15, 2341–2349, 2007.
49. Wang, M. Y., J. Xu, J. Wu, Y. Yan, and H.-L. Li, "FDTD study on scattering of metallic column covered by double-negative metamaterial," *Journal of Electromagnetic Waves and Applications*, Vol. 21, No. 14, 1905–1914, 2007.
50. Liu, X.-F., B. Z. Wang, and S.-J. Lai, "Element-free Galerkin method in electromagnetic scattering field computation," *Journal of Electromagnetic Waves and Applications*, Vol. 21, No. 14, 1915–1923, 2007.
51. Du, P., B. Z. Wang, H. Li, and G. Zheng, "Scattering analysis of large-scale periodic structures using the sub-entire domain basis function method and characteristic function method," *Journal of Electromagnetic Waves and Applications*, Vol. 21, No. 14, 2085–2094, 2007.
52. Tuz, V. R., "Three-dimensional Gaussian beam scattering from a periodic sequence of bi-isotropic and material layers," *Progress In Electromagnetics Research B*, Vol. 7, 53–73, 2008.
53. Sukharevsky, O. I. and V. A. Vasilets, "Scattering of reflector antenna with conic dielectric radome," *Progress In Electromagnetics Research B*, Vol. 4, 159–169, 2008.
54. Wang, M.-J., Z.-S. Wu, and Y. L. Li, "Investigation on the scattering characteristics of Gaussian beam from two dimensional dielectric rough surfaces based on the Kirchhoff approximation," *Progress In Electromagnetics Research B*, Vol. 4, 223–235, 2008.
55. Balanis, C. A., *Advanced Engineering Electromagnetics*, Wiley, New York, 1989.
56. Balanis, C. A., *Antenna Theory: Analysis and Design*, Wiley, New York, 1982.
57. Delves, L. M. and J. L. Mohamed, *Computational Methods for Integral Equations*, Cambridge University Press, Cambridge, 1985.
58. Babolian, E. and Z. Masouri, "Direct method to solve Volterra integral equation of the first kind using operational matrix with block-pulse functions," *Journal of Computational and Applied Mathematics*, Vol. 220, 51–57, 2008.
59. Burrus, C. S., R. A. Gopinath, and H. Guo, *Introduction to*

Wavelets and Wavelet Transforms, New Jersey, Prentice Hall, 1998.

60. Daubechies, I., *Ten Lectures on Wavelets*, SIAM, Philadelphia, 1992.
61. Aboufadel, E. and S. Schlicker, *Discovering Wavelets*, John Wiley & Sons, 1999.
62. Cattani, C., "Harmonic wavelets towards solution of nonlinear PDE," *Computers and Mathematics with Applications*, Vol. 50, 1191–1210, 2005.
63. Muniandy, S. V. and I. M. Moroz, "Galerkin modelling of the Burgers equation using harmonic wavelets," *Physics Letters A*, Vol. 235, 352–356, 1997.
64. Newland, D. E., "Harmonic wavelet analysis," *Proc. R. Soc. Lond. A*, Vol. 443, 203–222, 1993.
65. Cattani, C., "Connection coefficients of Shannon wavelets," *Mathematical Modelling and Analysis*, Vol. 11, No. 2, 1–16, 2006.
66. Cattani, C., "Shannon wavelet analysis," *Proceedings of the International Conference on Computational Science (ICCS)*, 982–989, 2007.
67. Bancroft, R., *Understanding Electromagnetic Scattering Using the Moment Method*, Artech House, London, 1996.